



**HAL**  
open science

## **Bi atoms mobility-driven circular domains at the Bi/InAs(111) interface**

M C Richter, J M Mariot, C M Gafoor, L Nicolai, O. Heckmann, U Djukic, W  
Ndiaye, I Vobornik, J Fujii, Nick Barrett, et al.

► **To cite this version:**

M C Richter, J M Mariot, C M Gafoor, L Nicolai, O. Heckmann, et al.. Bi atoms mobility-driven circular domains at the Bi/InAs(111) interface. *Surface Science: A Journal Devoted to the Physics and Chemistry of Interfaces*, 2016, 651, pp.147 - 153. 10.1016/j.susc.2016.03.032 . cea-01481529

**HAL Id: cea-01481529**

**<https://cea.hal.science/cea-01481529>**

Submitted on 2 Mar 2017

**HAL** is a multi-disciplinary open access archive for the deposit and dissemination of scientific research documents, whether they are published or not. The documents may come from teaching and research institutions in France or abroad, or from public or private research centers.

L'archive ouverte pluridisciplinaire **HAL**, est destinée au dépôt et à la diffusion de documents scientifiques de niveau recherche, publiés ou non, émanant des établissements d'enseignement et de recherche français ou étrangers, des laboratoires publics ou privés.



## Bi atoms mobility-driven circular domains at the Bi/InAs(111) interface



M.C. Richter<sup>a,b</sup>, J.-M. Mariot<sup>c,d,\*</sup>, M.A. Gafoor<sup>a</sup>, L. Nicolai<sup>a,e</sup>, O. Heckmann<sup>a,b</sup>, U. Djukic<sup>a</sup>, W. Ndiaye<sup>a</sup>, I. Vobornik<sup>f</sup>, J. Fujii<sup>f</sup>, N. Barrett<sup>b</sup>, V. Feyer<sup>g,h</sup>, C.M. Schneider<sup>g</sup>, K. Hricovini<sup>a,b</sup>

<sup>a</sup>Laboratoire de Physique des Matériaux et des Surfaces, Université de Cergy-Pontoise, 5 mail Gay-Lussac, 95031 Cergy-Pontoise, France

<sup>b</sup>DSM, IRAMIS, Service de Physique de l'Etat Condensé, CEA-Saclay, 91191 Gif-sur-Yvette, France

<sup>c</sup>Sorbonne Universités, UPMC Univ Paris 06, UMR 7614, Laboratoire de Chimie Physique–Matière et Rayonnement, 11 rue Pierre et Marie Curie, 75231 Paris Cedex 05, France

<sup>d</sup>CNRS, UMR 7614, Laboratoire de Chimie Physique–Matière et Rayonnement, 11 rue Pierre et Marie Curie, 75231 Paris Cedex 05, France

<sup>e</sup>Ludwig-Maximilians-Universität München, Department Chemie, Butenandtstraße 5–13, 81377 München, Germany

<sup>f</sup>Istituto Officina dei Materiali, TASC Laboratory, CNR, 34014 Trieste, Italy

<sup>g</sup>Peter Grünberg Institute (PGI-6) and JARA-FIT, Research Center Jülich, 52425 Jülich, Germany

<sup>h</sup>Sincrotrone Trieste S.C.p.A., NanoESCA Beamline, 34012 Basovizza, Trieste, Italy

### ARTICLE INFO

#### Article history:

Received 15 January 2016

Received in revised form 23 March 2016

Accepted 25 March 2016

Available online 19 April 2016

#### Keywords:

Indium arsenide

Bismuth

Chemical reactivity

Circular pattern morphology

PEEM

ARPES

### ABSTRACT

Bi films deposited on InAs(111) A and B sides have been studied by photoemission electron microscopy. A series of snapshots acquired during sequential annealing of the interfaces at temperatures below and above the melting temperature of Bi allowed obtaining a comprehensive image of the topographic and chemical evolutions of the Bi films that are found to be InAs side dependent. On the A side, a morphology of circular patterns controlled by Bi atoms mobility is observed. The patterns are formed on the pristine In-terminated InAs(111) surface covered by a weakly bonded Bi bilayer. On the B side, no particular morphology is observed due to a stronger chemical interaction between Bi and As atoms as evidenced by the spatially-resolved core-level photoelectron spectra.

© 2016 Elsevier B.V. All rights reserved.

### 1. Introduction

Bismuth is the heaviest group-V semimetal; so its large spin-orbit splitting combined with the loss of inversion symmetry at the surface may result in a band structure which is not spin degenerate [1]. It is therefore useful exploring how the electronic properties of bulk Bi are affected at the nanoscale, i.e. in Bi thin films deposited on semiconductors. Theoretical studies show the importance of one [2] or several [3] bilayers (BL) of Bi(111) for spin and topological systems [4–6].

This has motivated investigations of Bi thin films grown on various substrates, e.g. Si(111) [7, 8], SiC(0001) [9] and highly-oriented pyrolytic graphite [10]. InAs(111) is an alternative substrate that deserves to be investigated because of the close lattice match to Bi(111). Alloying of thin Bi films on As-terminated InAs(111) was analysed by core level photoelectron spectroscopy [11] and low-energy electron diffraction (LEED), revealing a complex chemistry

depending on the annealing temperature. However more detailed understanding of atomic arrangements, as obtained by combining local imaging and spectroscopy, is needed.

In this work, the structural, chemical and electronic properties of Bi thin films deposited on InAs(111) have been investigated using soft X-ray photoemission electron microscopy (PEEM). PEEM allowed us to get snapshots, in both real space and reciprocal space, of the clean surface and of the changes it undergoes after Bi deposition and upon annealing. We found that the nature of the InAs surface, i.e. either In-terminated (the so-called A side) or As-terminated (the B side), plays a crucial role in the Bi growth mode. A morphology of circular patterns controlled by Bi atoms mobility is observed on the A side. The B side shows no particularly organized morphology due to a stronger chemical interaction between Bi and As atoms.

### 2. Experimental

The substrates were cut from a 0.5 mm thick *n*-type InAs(111) wafer (Wafer Technology Ltd., UK) doped with S with a carrier concentration of  $3 \times 10^{18} \text{ cm}^{-3}$  and polished on both sides, one being

\* Corresponding author.

E-mail address: [jean-michel.mariot@upmc.fr](mailto:jean-michel.mariot@upmc.fr) (J.-M. Mariot).

cation (In) terminated, the A side, and the other anion terminated (As), the B side, due to the lack of inversion symmetry of the InAs crystal (see e.g. Ref. [12]). After degassing, both InAs(111)A and B surfaces were prepared by repeated cycles of ion bombardment ( $\text{Ar}^+$ , 600 eV) and annealing at 400 °C. Bismuth was deposited from a Knudsen cell at a rate of about 0.5 BL/min.

The experiments were performed at the NanoESCA beamline of the Elettra synchrotron radiation facility [13, 14]. The NanoESCA instrument combines an electrostatic lens and a double-pass hemispherical electron analyser allowing work function overview imaging in real time using the 4.9 eV photons emitted by a mercury arc lamp (achieved lateral resolution 50 nm). Using synchrotron radiation (*p*-polarised light) both element specific images and small-spot chemical state images can be recorded by photoelectron spectroscopy; *k*-space imaging by angle-resolved photoelectron spectroscopy (ARPES) can be done as well. The ARPES spectra were taken with a photon energy  $h\nu$  of 43 eV, as well as most Bi 5*d* and In 4*d* PEEM images; some In 3*d*, As 4*d* and Bi 5*d* core level PEEM images were recorded at  $h\nu = 100$  eV. The spatial resolution was better than 1  $\mu\text{m}$ . The energy resolution was  $\approx 0.3$  eV. All measurements have been made at room temperature.

### 3. Results and discussion

#### 3.1. Clean InAs(111) surfaces

Typical LEED patterns and ARPES data for the InAs(111) A and B sides after the above-mentioned surface preparation are shown in Fig. 1 (a) and in Fig. 1 (b and c), respectively (note that throughout this article, blue and orange colours are used in the figures for real- and reciprocal-space representations, respectively, except for the LEED pictures). The LEED patterns show a  $(2 \times 2)$  reconstruction [Fig. 1 (a), top view] for the A side and a non-reconstructed surface for the B side [Fig. 1 (a), bottom view], in agreement with previously reported investigations (see e.g. Ref. [15] and the references cited therein).

Identical electron energy bands in the  $\bar{\Gamma}$ - $\bar{M}$  direction are observed for both sides. As an example we give in the bottom panel of Fig. 1 (c) an ARPES spectrum that is typical of the A side. The bands are in agreement with previously published ARPES spectra [16].

The surface crystallography of the A and B sides is also revealed by the *k*-maps recorded [Fig. 1 (c)] very close to the Fermi energy ( $E_F$ ) because of the presence of an electron accumulation layer in the vicinity of the  $\bar{\Gamma}$  point for both surfaces. For the A side, the periodic variation of the spectral weight near  $E_F$  [see the dash-dotted (red) line in Fig. 1 (c), bottom panel] along the  $\bar{\Gamma}$ - $\bar{M}$  direction is given in the top panel of Fig. 1 (c): the intense and faint (marked by the black arrows) peaks correspond to the accumulation layer observed at  $\bar{\Gamma}$  for the  $(2 \times 2)$  reconstruction. This accumulation layer was observed for the first time on InAs surfaces by Olsson et al. [16] and later investigated in detail by King et al. [17]. The corresponding two-dimensional *k*-map is given at the top of Fig. 1 (b): it shows a strong hexagonal pattern with additional weaker spots corresponding to the  $(2 \times 2)$  reconstruction; two black arrows are used as a guide to the eye for the additional spots of this pattern. For the B side, only the hexagon associated with the unreconstructed surface is visible [bottom panel of Fig. 1 (b)].

The analysis of the In 4*d* and As 3*d* core level photoelectron spectra reveals the same components as those previously reported in Refs. [11, 18, 19]; thus these spectra are not shown here.

#### 3.2. Bi/InAs(111) interfaces

Bismuth was then deposited on such prepared A and B sides. Epitaxial growth on the A side leads to a high-quality Bi monocrystal already after deposition of several BL of Bi whereas, for the same

coverage, the B surface induces formation of islands. However, after deposition of  $\approx 30$  BL the crystal quality is almost the same for both sides. For this reason, films with this thickness were initially prepared for our studies.

As an example, we show in Fig. 2 the results for the deposition on the B side. The mercury lamp image shows a “granularity” on a scale of 1  $\mu\text{m}$ . More quantitative information can be obtained from a pixel by pixel fit to the threshold spectra across the whole field of view. The photoemission threshold is fitted using an error function and the result is mapped in Fig. 2 (a). The histogram of the work function distribution shown in the inset to Fig. 2 (a) is centred on 4.37 eV with a full width at half maximum of 50 meV. This is a strong evidence for a chemically uniform surface. The measured work function value in PEEM has to be corrected for the Schottky effect due to the high extractor field [20]. In this case 98 meV should be added to the measured values, thus the true work function is 4.47 eV, close to the value of 4.32 eV measured by ultra-violet photoelectron spectroscopy [21] for Bi(001). We have a more dense (111) surface which should indeed show a higher work function than the (001) surface. Typical values of the work function fluctuation are 0.1–0.4 eV. The nearly uniform work function across the field of view suggests that the contrast is rather of topographical nature. This is confirmed by scanning tunnelling microscopy (STM), which shows [see Fig. 2 (b)] six-fold symmetry patterns at a scale of  $\sim 100$  nm corresponding to Bi(111) terraces. This observation is very similar to the one done on films of  $\text{Bi}_2\text{Se}_3$  (which has the same crystalline structure as Bi) grown by molecular beam epitaxy on  $\text{SrTiO}_3(111)$  substrates [22]. The STM image [Fig. 2 (c)] shows a perfect hexagonal arrangement of closed-packed Bi atoms, without any presence of allotrope structures. Those may appear in initial stages of growth, as this is the case for the Bi/Si(111) interface [23]. The excellent crystallinity of the terraces is also confirmed by the sharp Bi/InAs(111)- $(1 \times 1)$  LEED pattern [Fig. 2 (d)] as well as by the well-defined energy bands and Fermi surface obtained by ARPES [Fig. 2 (e) and (f), respectively] that are identical to those observed for the (111) surface of bulk bismuth (see e.g. Refs. [24–26]). One can recognize the hexagonal electron pocket at the centre of the Fermi surface, surrounded by six “petal” hole pockets along the  $\bar{\Gamma}$ - $\bar{M}$  directions.

#### 3.3. Annealed Bi/InAs(111)A interface

The deposited films were then annealed. We stepwise increase the temperature, looking at the surface morphology by recording at each step the PEEM image matrix over the threshold-close valence band with the mercury lamp. An important change in the images starts to appear at an annealing temperature of  $\approx 230$  °C [see Fig. 3 (a)]. This is not unexpected because this temperature is close to the melting point of bismuth, which means that the mobility of Bi atoms is then greatly enhanced, some evaporation not being excluded. One notes that the long-range homogeneity observed in Fig. 2 (a) has been broken and that small terraces of the original surface gain in size, spanning now a few 100  $\mu\text{m}^2$ . The work function analysis after annealing at 230 °C is shown in Fig. 3 (a). The majority of the surface has a work function of 4.28 eV, whereas the darker geometric patches have a work function of 4.33 eV. This can also be seen from the broader histogram of work function values [see the inset to Fig. 3 (a)].

At the same time, the observed modification due to the enhanced mobility of Bi atoms does not alter the crystal quality of the remaining film because the large terraces still retain the six-fold symmetry. This is further demonstrated in Fig. 3 (b and c) showing that the film has the all-over characteristics of the electronic band structure and of the Fermi surface of Bi(111) [see also Fig. 2 (e and f) for comparison]. So, the thickness of the terraces must be large enough to stand for a bulk crystal and the structure is that of the original film.

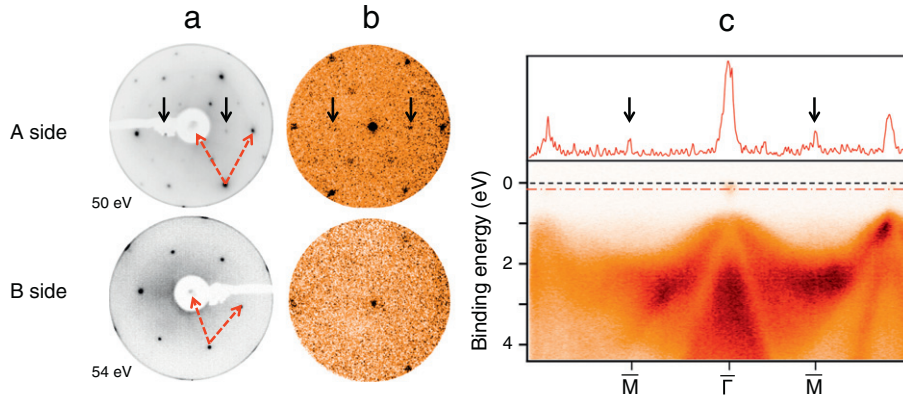


**Fig. 1.** Clean InAs(111): (a) LEED patterns (at 50 eV for the A side and at 54 eV for the B side). The basis vectors of the reciprocal space are shown as dashed (red) arrows; (b) *k*-maps near the Fermi level; (c) ARPES of the A side along the  $\bar{\Gamma}$ - $\bar{M}$  direction (bottom panel) and intensity profile of the ARPES spectrum near (red dash-dotted line) the Fermi level (black dashed line) (top panel).

The annealing brings as well other new features with it. In the middle of the terraces one remarks small white triangular regions that can be attributed to the formation of Bi clusters as will be proven by Bi 5*d* core level PEEM. This is better seen in Fig. 3 (d), which is the energy filtered work function image at  $E - E_F = 4.7$  eV of the region shown on the work function map by a white frame [Fig. 3 (a)]. Here we have chosen  $E - E_F$  such that the thickness of the Bi layer scales the darkness of the blue colour. In all other figures [Fig. 3 (e–g)] corresponding to PEEM images recorded at the maximum intensity of the In 4*d*, As 3*d* and Bi 5*d* photoelectron signals the white shadows are observed as well. One can also remark that the white triangles are present only on the thinner Bi terraces (light blue colour in the work function image). Clearly, at the given annealing temperature and due to higher atom mobility, bismuth has the tendency to deplete the surface of the substrate and agglomerate in clusters.

Another proof of cluster formation is the fact that the triangles have the same orientation in the core-level PEEM images, but a different one in the mercury lamp image. This is simply due to the fact that the incoming light shines on the sample in a different azimuth for each type of picture while the angle of incidence for the mercury lamp radiation and for the synchrotron radiation is the same with

respect to the surface normal. We attribute these white triangles to the drop shadow (absence of photoemission intensity) resulting from the presence of clusters, as the triangles exist in the same place whatever the core-level or valence-band energy-filtered PEEM image is considered. Moreover, a closer inspection of element-sensitive images in Fig. 3 (e–g) reveals the presence of Bi clusters appearing as small dark dots at the upper part of the triangles in Fig. 3 (g).

When going from Fig. 3 (d) to Fig. 3 (e and f), the contrast is reversed, testifying the presence of In and As in about the same proportion on the light blue central terrace of Fig. 3 (d). Note that the slight variation of photoemission intensity across the terrace is due to an inhomogeneity of the synchrotron light and not to a concentration gradient across the sample. The contrast is again reversed in Fig. 3 (g), measured at the maximum of the Bi 5*d*<sub>5/2</sub> core level photoemission, indicating a small concentration of bismuth inside the terrace, except on the spots above the white triangles, as discussed above. On the contrary, outside the terrace, there is a massive Bi signal, corroborating our attribution of Bi film thickness in the various regions.

Raising the annealing temperature to 300 °C, i.e. above the melting temperature of Bi, switches the atom dynamics to another regime

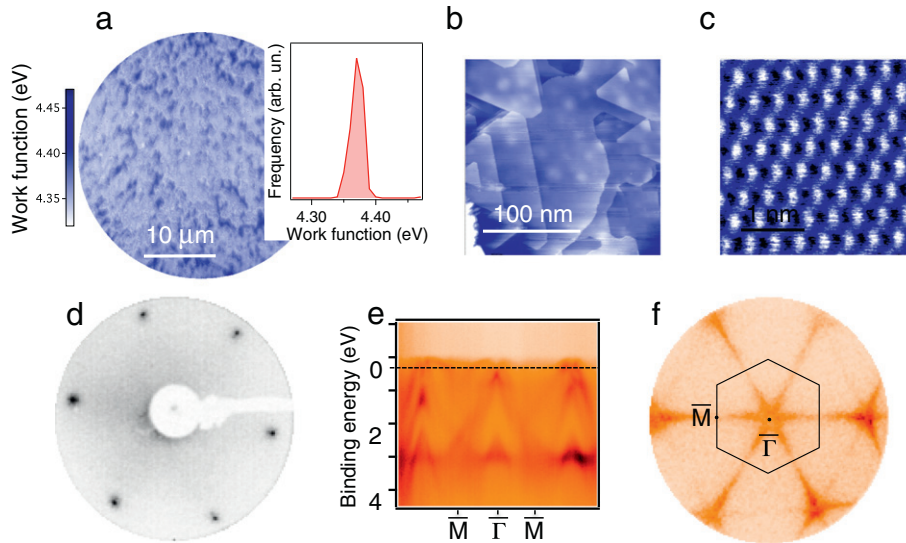


**Fig. 2.** 30 BL Bi/InAs(111)B: (a) work function map taken with the mercury lamp and work function histogram (inset); (b) STM image showing terraces with a six-fold symmetry; (c) STM image showing the hexagonal arrangements of the Bi atoms on a terrace; (d) Bi/InAs(111)B-(1 × 1) LEED pattern (at 33 eV); (e) ARPES in the  $\bar{\Gamma}$ - $\bar{M}$  direction; (f) Fermi surface [the Bi(111) surface Brillouin zone with relevant high symmetry points is shown for reference].

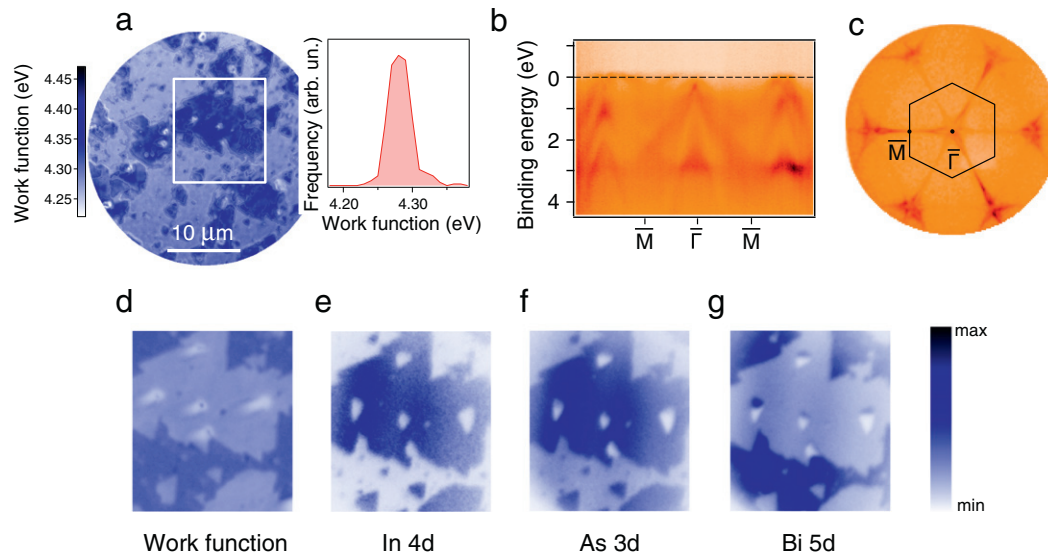


**Fig. 3.** 30 BL Bi/InAs(111)A sample after annealing at 230 °C: (a) work function map taken with the mercury lamp and work function histogram; (b) ARPES in the  $\bar{\Gamma}$ - $\bar{M}$  direction; (c) Fermi surface [the Bi(111) surface Brillouin zone with relevant high symmetry points is shown for reference]; (d) work function image for the region indicated by the white frame in (a); (e–g) In 4d, As 3d and Bi 5d PEEM corresponding energy filtered images of the white frame area.

and affects significantly the topography of the surface. The first qualitative observation on the work function map [Fig. 4 (a)] indicates that the domains with six-fold symmetry have been replaced by an array of micrometer-sized circular patches with a spot at their centre. Upon repeated annealing at the same temperature, each of them during about 10 min, the patches decrease in size as well as in density, until complete disappearance, only the central spots staying in place [see Fig. 4 (b and c)]. The work function histograms

obtained after successive annealings are shown in Fig. 4 (d). After the first annealing most of the surface has a work function centred on 4.24 eV, lower than that of as grown Bi but still close to the value reported in the literature for Bi. A significantly higher value of 4.50 eV is observed in the round patches, pointing to a distinct surface chemistry. The latter is extinguished after the second annealing and the main work function peak shifts to 4.30 eV and finally 4.44 eV after the third annealing. The corresponding ARPES data,

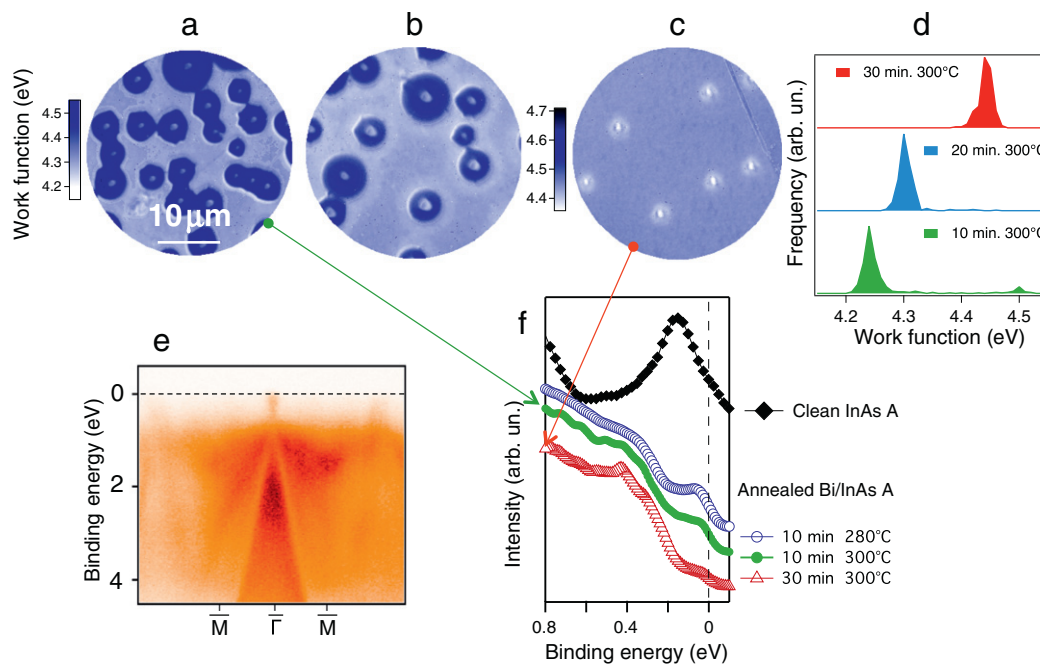


**Fig. 4.** 30 BL Bi/InAs(111)A sample after annealing at 300 °C: (a) work function map taken with the mercury lamp after a first 10 min annealing; (b) and (c) further annealing for 10 and 20 min, respectively; (d) work function histograms corresponding to samples (a–c); (e) ARPES spectrum in the  $\bar{\Gamma}$ - $\bar{M}$  direction of the surface shown in (a); (f) energy distribution curve close to the Fermi level for the surfaces in (a) and (c). For comparison, the spectra corresponding to the clean InAs(111)A surface and to the 30 BL Bi/InAs(111)A surface annealed at 280 °C are also shown.

averaged over the whole image [Fig. 4 (e)], reveal that the band structure is no more that of bismuth but is related to that of InAs as also testified by a clear signature of the accumulation layer [see Fig. 1 (c) for comparison]. The evolution of the ARPES spectrum can be more precisely followed through the energy distribution curve at the  $\bar{\Gamma}$  point. In Fig. 4 (f) we plot the energy distribution curves corresponding to the images shown in Fig. 4 (a) and (c). For reference, we show also the energy distribution curve of the Bi/InAs(111)A surface annealed at 280 °C and that of the clean InAs(111)A surface. One can see that the intensity of the feature due to the accumulation layer decreases when going from the InAs(111)A surface to the most annealed Bi/InAs(111)A surface. At the same time, the band dispersion in 2-dimensional ARPES data loses in contrast (not shown). This leads to the first qualitative conclusion that the annealing above the melting temperature of bismuth progressively destroys the crystallinity of the surface.

In order to identify the chemical nature of each of the three different regions in Fig. 4 (a), i.e. the circular patches, the spots at their centre and the inter-patch region, we acquired the PEEM images over the core level spectra and show the images at the maximum intensity of the In  $4d_{5/2}$  and Bi  $5d_{5/2}$  core level spectra [Fig. 5 (a and b), respectively].

The In concentration is high on the circular patches, but low on the central spots [Fig. 5 (a)]. Bismuth has a lower concentration on the patches than between them. The Bi concentration is also high in the central spots, indicating that those are made of bismuth clusters which we already observed in Fig. 3. This is also corroborated by the white shadows just below the Bi spots [Fig. 5 (b)]. From the size of the shadow and from the angle between the direction of the impinging photons and the sample surface ( $\approx 25^\circ$ ), we estimate the height of the Bi clusters to be  $\approx 250$  nm.

The core-level chemical shifts [see Fig. 5 (c and d)] greatly help to better understand the morphology of the annealed surfaces. The shape and the binding energy of the Bi  $5d_{5/2}$  photoemission from the central spot can be considered as corresponding to bulk Bi and is taken here as a reference [spectrum in green with triangles in

Fig. 5 (d)]. When going from the spot to the circular patch, the concentration of bismuth strongly decreases and the core level is shifted to lower binding energies.

This area of the patches is typical of a situation where Bi forms an interface with the In-terminated surface of InAs: Bi atoms interact weakly with In and a shift of the Bi core level to lower binding energy occurs as this is the case for the Bi/InAs(100) surface (see Ref. [27] and the references cited therein). The photoemission spectra and the calculations reported in this publication lead to the conclusion that when annealing Bi films on an In-rich surface, the most stable atomic model of the interface consists of one BL of Bi in contact with the In surface layer. This implicitly means in our case that the remaining amount of bismuth migrates to form clusters as soon as the temperature is high enough. As we will explain, the formation of circular patches is a logical consequence of this. We suggest that the circular patches consist of the InAs(111)A monocrystal covered by one BL of bismuth. This suggestion also agrees with the fact that prolonged annealing destroys the crystallinity of the substrate which is in fact observed as a progressive reduction of the number of patches, a diminution of their size and the disappearance of the accumulation layer, in complete consistency with Fig. 4.

Now, the question concerning the structure of the region in between the patches needs to be addressed. In this region, the Bi  $5d_{5/2}$  core level shifts to higher binding energies, which is a fingerprint of bonding between Bi and As [11]. This is a logical consequence of the prolonged annealing at 300 °C which provides enough energy to stimulate the formation of Bi–As bonds which are stronger than Bi–In bonds, as testified for instance by core-level shifts [11, 27]. This can only be done if the uppermost In layer is broken favouring the diffusion of As atoms to the surface, which is consistent with a progressive loss of crystal quality.

This scenario is the last missing argument to complete our explanation of the observed surface morphology. First of all, it is important to keep in mind that our PEEM images are measured at room temperature and therefore show a frozen atomic configuration of the surface at higher temperatures. Our results indicate that during the annealing at temperatures slightly above the melting point of Bi, the major part of the surface formed by one Bi BL sitting on the In top layer is preserved and, at the same time, in arbitrarily scattered (homogeneously distributed) points of the surface, probably where defects are present, a formation of Bi–As compounds is initiated. This necessitates more Bi atoms than available in one Bi bilayer and the Bi reservoirs are the clusters which were formed during the annealing of the film. The reaction between Bi and As is then fuelled by a flux of mobile Bi atoms leaving the cluster and sliding on top of the Bi bilayer which is sticking to the surface. As the flux of atoms is isotropic, the patches maintain a circular shape with the cluster in their centre. Implicitly, the rate of the reaction between Bi and As is lower than the velocity of surface-melted Bi atoms. Prolonged annealing favours a progressive advance of the frontier between an amorphous-like mixture of Bi–As–In compounds and the pristine InAs crystal covered by one Bi bilayer.

### 3.4. Annealed Bi/InAs(111)B interface

Annealings leave the B side morphology completely different from the one of the A side, as observed on the Bi  $5d_{5/2}$  and In  $4d$  PEEM images [see Fig. 6 (a and b), respectively]. The surface is inhomogeneous, with scattered spots, and the ARPES measurement shows only fuzzy InAs-like bands (not shown here).

As seen in Fig. 6 (a), we observe a higher density of Bi clusters of smaller size as compared to the A side. Again, the white shadows underneath the clusters are a proof of their height which can be estimated to be at least a quarter of their diameter ( $\lesssim 1 \mu\text{m}$ ). As expected, on the clusters, the Bi  $5d_{5/2}$  photoelectron spectrum [red curve with dots of Fig. 6 (c)] corresponds mainly to bulk Bi. In between

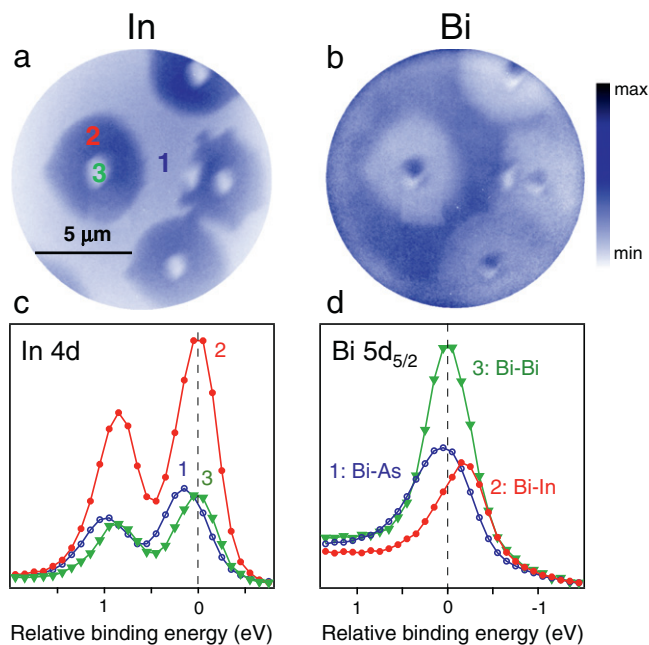


**Fig. 5.** 30 BL Bi/InAs(111)A sample after a 10 min annealing at 300 °C: (a) In  $4d$  and (b) Bi  $5d$  PEEM images; (c) In  $4d$  and (d) Bi  $5d_{5/2}$  photoelectron spectra corresponding to the regions 1, 2 and 3 of (a).

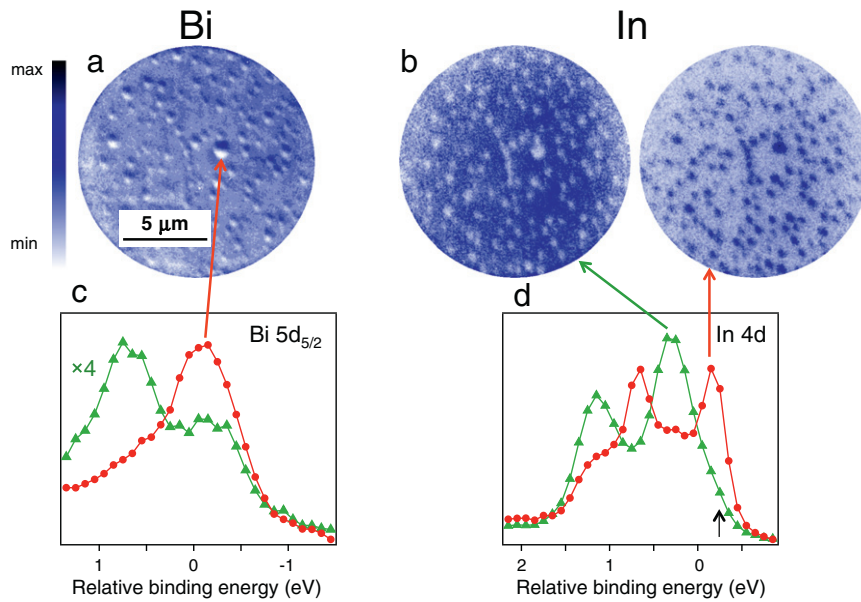


**Fig. 6.** 30 BL Bi/InAs(111)B sample after 10 min annealing at 300 °C: (a) Bi PEEM image averaged over the whole Bi  $5d_{5/2}$  photoelectron spectrum; (b) In PEEM image recorded at the energy of the intensity maximum of the In  $4d$  photoelectron spectrum, between the clusters (left) and on the clusters (right); (c) and (d) Bi  $5d_{5/2}$  and In  $4d$  core level spectra for two regions: between the Bi clusters (green curve with triangles) and on the Bi clusters (red curve with dots).

the clusters we find an added component with a chemical shift of  $\approx 1$  eV to higher binding energies [green curve with triangles in Fig. 6 (c)] which is attributed to Bi–As bonds [11]. The In  $4d$  photoelectron spectra differ significantly whether they are recorded either on (red curve with dots) or between (green curve with triangles) the clusters [see Fig. 6 (c and d), respectively]. PEEM images in Fig. 6 (b) nicely show that the In  $4d$  intensity contrast is reversed in these two regions. Between the clusters, the In  $4d$  spectrum is similar to that encountered for low Bi deposition ( $\lesssim 3$  BL) on InAs, as reported in Ref. [11]. Namely, we observe [see the arrow in Fig. 6 (d)] a shoulder at  $\approx 0.3$  eV on the low binding energy side of the main peak attributed to Bi–In bonds. Clearly, on the clusters, this component is strongly enhanced because here only Bi–In bonds can be present. These bonds contribute to the main component seen in the Bi  $5d_{5/2}$  spectrum of Fig. 6 (c) (red curve with dots), as the Bi–In and Bi–Bi bond binding energies are barely distinguishable [11]. This is in line with the studies reporting formation of ternary InAs $_{1-x}$ Bi $_x$  alloys with Bi substituting As and giving thus a possible explanation for the Bi–In bonds [28].

#### 4. Conclusions

We observe a clear difference in morphology of Bi films when grown and then annealed on the In-terminated (A side) and As-terminated (B side) of the InAs(111) surface. After the deposition of a thick film ( $\approx 30$  BL), a high-quality Bi monocrystal is built up on both A and B sides.

Annealing of the interface on the A side leads to two different regimes that depend on the temperature. Interestingly, the temperature that exceeds slightly the Bi melting point switches the atom dynamics to a regime that affects significantly the topography of the surface. The six-fold symmetry terraces of the original monocrystal are replaced by an array of micrometer-sized circular patches with a Bi cluster in the middle. We identify the patches with pristine InAs(111)A covered with one Bi bilayer. In between the patches, ternary Bi–In–As compounds are formed having no long-distance crystalline order. High-mobility Bi atoms flowing from the central

cluster and fuelling Bi–In–As compounds formation control the reaction front between these two regions. The isotropic flux of atoms guarantees the circular shape of the patches.

The observed mechanism leading to this morphology of circular patterns opens a way to controlled surface patterning of semiconductor interfaces. The thickness of the originally deposited film and the temperature and duration of annealing can be used to define the size and the density of the circular patterns.

The situation on the InAs B side is quite different. After annealing at 300 °C, the surface presents less order than for the A side and Bi clusters are formed with an irregular distribution in size. The origin of this difference can be explained by a stronger chemical bonding between Bi and the As-terminated B side. This induces a more complex structure at the interface, inhibiting the mobility of Bi atoms during the annealing.

#### Acknowledgement

The research leading to these results has received funding from the European Community's Seventh Framework Programme (FP7/2007–2013) under grant agreement n°312284.

#### References

- [1] S. Agergaard, Ch. Søndergaard, H. Li, M.B. Nielsen, S.V. Hoffmann, Z. Li, Ph. Hofmann, *New J. Phys.* 3 (2001) 15.
- [2] M. Wada, S. Murakami, F. Freimuth, G. Bihlmayer, *Phys. Rev. B* 83 (2011) 121310(R).
- [3] Z. Liu, C.-X. Liu, Y.-S. Wu, W.-H. Duan, F. Liu, J. Wu, *Phys. Rev. Lett.* 107 (2011) 136805.
- [4] M.Z. Hasan, C.L. Kane, *Rev. Mod. Phys.* 82 (2010) 3045.
- [5] X.-L. Qi, S.-C. Zhang, *Rev. Mod. Phys.* 83 (2011) 1057.
- [6] Y. Ando, *J. Phys. Soc. Jpn.* 82 (2013) 102001.
- [7] A. Takayama, T. Sato, S. Souma, T. Takahashi, *Phys. Rev. Lett.* 106 (2011) 166401.
- [8] A. Takayama, T. Sato, S. Souma, T. Oguchi, T. Takahashi, *Nano Lett.* 12 (2012) 1776.
- [9] H. Huang, S.L. Wong, Y. Wang, J.-T. Sun, X. Gao, A.T.S. Wee, *J. Phys. Chem. C* 118 (2014) 24995.
- [10] P.J. Kowalczyk, O. Mahapatra, D.N. McCarthy, W. Kozłowski, Z. Klusek, S.A. Brown, *Surf. Sci.* 605 (2011) 659.

- [11] K. Szamota-Leandersson, M. Leandersson, M. Göthelid, U.O. Karlsson, Surf. Sci. 605 (2011) 12.
- [12] E.T. Yu, III-V Nitride semiconductors, in: E.T. Yu, M.O. Manasreh (Eds.), *Optoelectronic Properties of Semiconductors and Superlattices*, Vol. 16, Taylor & Francis, New York, 2003, Ch. 4, p. 161.
- [13] C. Wiemann, M. Patt, I.P. Krug, N.B. Weber, M. Escher, M. Merkel, C.M. Schneider, e-J. Surf. Sci. Nanotech. 9 (2011) 395.
- [14] C.M. Schneider, C. Wiemann, M. Patt, V. Feyer, L. Plucinski, I.P. Krug, M. Escher, N. Weber, M. Merkel, O. Renault, N. Barrett, J. Electron Spectrosc. Related Phenom. 185 (2012) 330.
- [15] E. Hilner, E. Lundgren, A. Mikkelsen, Surf. Sci. 604 (2010) 354.
- [16] L.Ö. Olsson, L. Ilver, J. Kanski, P.O. Nilsson, C.B.M. Andersson, U.O. Karlsson, M.C. Håkansson, Phys. Rev. B 53 (1996) 4734.
- [17] P.D.C. King, T.D. Veal, C.F. McConville, J. Zúñiga Pérez, V. Muñoz Sanjosé, M. Hopkinson, E.D.L. Rienks, M.F. Jensen, Ph. Hofmann, Phys. Rev. Lett. 104 (2010) 256803.
- [18] K. Szamota-Leandersson, M. Göthelid, O. Tjernberg, U.O. Karlsson, Appl. Surf. Sci. 212–213 (2003) 589.
- [19] P. Palmgren, K. Szamota-Leandersson, J. Weissenrieder, T. Claesson, O. Tjernberg, U.O. Karlsson, M. Göthelid, Surf. Sci. 574 (2005) 181.
- [20] O. Renault, R. Brochier, A. Roule, P.-H. Haumesser, B. Krömker, D. Funnemann, Surf. Interface Anal. 38 (2006) 375.
- [21] H. Kakuta, T. Hirahara, I. Matsuda, T. Nagao, S. Hasegawa, N. Ueno, K. Sakamoto, Phys. Rev. Lett. 98 (2007) 247601.
- [22] J. Chen, H.J. Qin, F. Yang, J. Liu, T. Guan, F.M. Qu, G.H. Zhang, J.R. Shi, X.C. Xie, C.L. Yang, K.H. Wu, Y.Q. Li, L. Lu, Phys. Rev. Lett. 105 (2010) 176602.
- [23] T. Nagao, J.T. Sadowski, M. Saito, S. Yaginuma, Y. Fujikawa, T. Kogure, T. Ohno, Y. Hasegawa, S. Hasegawa, T. Sakurai, Phys. Rev. Lett. 93 (2004) 105501.
- [24] C.R. Ast, H. Höchst, Phys. Rev. Lett. 87 (2001) 177602.
- [25] T. Hirahara, T. Nagao, I. Matsuda, G. Bihlmayer, E.V. Chulkov, Yu. M. Koroteev, P.M. Echenique, M. Saito, S. Hasegawa, Phys. Rev. Lett. 97 (2006) 146803.
- [26] Ph. Hofmann, Prog. Surf. Sci. 81 (2006) 191.
- [27] M. Ahola-Tuomi, M.P.J. Punkkinen, P. Laukkanen, M. Kuzmin, J. Lång, K. Schulte, A. Pietzsch, R.E. Perälä, N. Räsänen, I.J. Väyrynen, Phys. Rev. B 83 (2011) 245401.
- [28] Prabhat Verma, K. Oe, M. Yamada, H. Harima, M. Herms, G. Imer, J. Appl. Phys. 89 (2001) 1657.